

ARTICLE

Quantitative Surface Chirality Detection with Sum Frequency Generation Vibrational Spectroscopy: Twin Polarization Angle Approach[†]

Feng Wei^a, Yan-yan Xu^{b,‡}, Yuan Guo^b, Shi-lin Liu^a, Hong-fei Wang^{b,*}*a* Hefei National Laboratory for Physical Sciences at Microscale, Department of Chemical Physics, University of Science and Technology of China, Hefei 230026, China*b* Beijing National Laboratory for Molecular Sciences, Laboratory of Molecular Reaction Dynamics, Institute of Chemistry, Chinese Academy of Sciences, Beijing 100190, China

(Dated: Accepted on December 6, 2009)

Here we report a novel twin polarization angle (TPA) approach in the quantitative chirality detection with the surface sum-frequency generation vibrational spectroscopy (SFG-VS). Generally, the achiral contribution dominates the surface SFG-VS signal, and the pure chiral signal is usually two or three orders of magnitude smaller. Therefore, it has been difficult to make quantitative detection and analysis of the chiral contributions to the surface SFG-VS signal. In the TPA method, by varying together the polarization angles of the incoming visible light and the sum frequency signal at fixed s or p polarization of the incoming infrared beam, the polarization dependent SFG signal can give not only direct signature of the chiral contribution in the total SFG-VS signal, but also the accurate measurement of the chiral and achiral components in the surface SFG signal. The general description of the TPA method is presented and the experiment test of the TPA approach is also presented for the SFG-VS from the S- and R-limonene chiral liquid surfaces. The most accurate degree of chiral excess values thus obtained for the 2878 cm⁻¹ spectral peak of the S- and R-limonene liquid surfaces are (23.7±0.4)% and (-25.4±1.3)%, respectively.

Key words: Sum-frequency generation vibrational spectroscopy, Twin polarization angle approach, Surface, Chirality, Limonene

I. INTRODUCTION

Second order nonlinear techniques, such as the surface second harmonic generation (SHG) and surface sum-frequency generation vibrational spectroscopy (SFG-VS), have shown to be the effective probe of surface molecular chirality [1–9]. This is not only because SHG and SFG-VS are intrinsically interface specific processes which can selectively probe the interfacial molecules with submonolayer sensitivity [10–13], but also because the third-rank second order nonlinear optical susceptibility tensors can uniquely describe the intrinsic steric chiral interactions between the chiral

molecule and the optical fields [6,14].

In contrast to SHG and SFG-VS, the common linear optical techniques, such as the circular dichroism (CD) spectroscopy, optical rotatory dispersion (ORD), vibrational circular dichroism (VCD), vibrational Raman optical activity (ROA), have neither the surface selectivity nor the monolayer sensitivity [15–21].

Since the biological molecules in nature are consisted with only left-handed amino-acids and right-handed sugars, as well as double helix DNA and RNA molecules, SHG and SFG-VS have tremendous potential in understanding the chiral structure and chiral recognition at molecular surfaces and in the biological membranes. One of the key limitation for the application of the SHG and SFG-VS techniques for such studies lies in how accurate and quantitative the experimental measurement and data analysis can be achieved. The past few years have witnessed the developments of the quantitative measurement and analysis in surface SHG and SFG-VS studies [22,23]. These developments was based on the extensive use of polarization and experimental configuration control in designing SHG and SFG-VS experiments and in SHG and SFG-VS data analysis [9,24–35], and also based on the unified treatment and analysis of the macroscopic susceptibility tensors in relationship to the microscopic molecular tensors

[†]Part of the special issue for “the Chinese Chemical Society’s 11th National Chemical Dynamics Symposium”.

[‡]Also graduate student of the Graduate University of the Chinese Academy of Sciences. Current address: Laboratory of Soft Matter Physics, Institute of Physics, Chinese Academy of Sciences, Beijing 100190, China.

*Author to whom correspondence should be addressed. Current address: Environmental Molecular Science Laboratory, Pacific Northwest National Laboratory, 902 Battelle Boulevard, P.O. Box 999, MSIN K8-91, Richland, WA 99352, U.S.A. E-mail: hongfei.wang@pnl.gov; Tel.: +1-509-3716717; Fax: +1-509-3716445.

[22,23,36,37]. Therefore, extending these ideas and developments into chiral surface measurement and analysis is naturally a step forward in the related fields.

In theory, if the experimental data can be obtained with all the possible combination of the polarizations as well as experimental configurations, the relative or absolute values of all the experimental measurable nonlinear susceptibility tensor elements can be accurately obtained [34,35]. However, the application of this approach may be limited since it requires conducting complicated sets of experiments and performing overwhelming data collection and analysis. Most important of all, the physical meanings and pictures of the SHG and SFG-VS contributions may not be ready to be explicitly revealed until the analysis of huge amount of data has been carried out. Particularly, in the process for multi-parameter fitting of the huge amount of polarization data sets, the uncertainty of the contributions to the SHG or SFG-VS signal from the much smaller terms may be subject to significant errors. As shown in recent polarization dependent SHG and SFG-VS studies, not all polarization dependent measurements are equal in terms of experimental uncertainty and thus in favor of accuracy for the data fitting [9,22,23,30]. As we have known that in SHG and SFG-VS, the values of the chiral terms are usually two orders of magnitude smaller than the values of the achiral terms [5,6,38–40]. Therefore, the search of methodology for simpler but necessary measurements which are sensitive and accurate to determine the relatively smaller chiral terms, is always desired for complicated techniques such as SHG and SFG-VS [9,22,23]. Otherwise, whether the surface is chiral may not even be able to be determined [9,41–43].

In a recent study [9], we found that in surface chiral measurement with SHG-linear dichroism (SHG-LD), the degree of chiral excess (DCE) of the interface or film as defined below [44] can be accurately determined by performing the SHG-LD experiment with the detection polarization of the second harmonic signal fixed at the s-polarization, *i.e.* the optical field is perpendicular to the incident plane formed with the incident light beam and the surface normal, while the polarization of the incoming fundamental light beam is varied from 0° to 360° . In this way, not only the chiral contribution from the surface molecules was explicitly identified by the difference of the SHG signal on this so-called s-polarization detection curve at the 45° and -45° (or 135°), but also the small chiral term was accurately determined and the uncertainty for the DCE value, which quantifies the chiral excess of the surface, thus was determined as small as 1%.

$$\text{DCE} = \frac{\Delta I}{I} = \frac{2(I_{-45^\circ} - I_{+45^\circ})}{I_{-45^\circ} + I_{+45^\circ}} \quad (1)$$

With such accuracy in determination of the surface DCE values established with the s-polarization detec-

tion in the SHG-LD, we showed that the chirality of the Langmuir monolayer formed with the achiral PARC18 (5-octadecyloxy-2-(2-pyridylazo)phenol) molecule is inhomogeneous in nature, and the chirality formation was due to molecular self-assemble instead of lateral compression induced [9,42].

With such development in the SHG-LD detection, we started looking for the SFG-VS-LD detection schemes which are equivalent to the s-polarization detection in SHG-LD. In order to make SFG-VS-LD measurement with similar accuracy and explicitness for surface chiral detection as the s-polarization detection in the SHG-LD, the polarizations of two out of the three optical fields in the SFG experiment need to be varied in a collaborative fashion. In the SHG-LD experiment, when the polarization of the incoming optical field was varied, the two fundamental photons that generated the SHG photon were with the same polarization. This simple fact made the s-polarization detection curve uniquely sensitive for detection of the small chiral terms in the SHG-LD. To make the SFG-VS-LD work like SHG-LD, the polarizations of two out of the three optical fields has to be the same or to differ with a fixed value. Therefore, we call this scheme as the twin-polarization angle (TPA) approach.

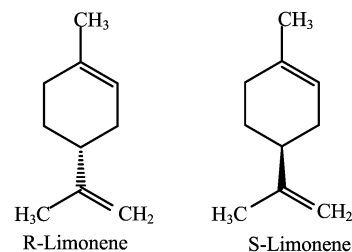


FIG. 1 Molecular structure of R-limonene and S-limonene.

In this work, we present the theoretical descriptions of the TPA approach in the SFG-VS-LD measurement. Results show that the SFG-VS-LD measurement for the S- and R-limonene chiral liquid surfaces using this TPA method indeed followed the descriptions, and the surface DCE value from these two surface can be explicitly and accurately determined. We believe this development in measurement accuracy is going to pave the way for accurate measurement of chiral interactions and chiral recognition of the molecular surfaces as well as biological membranes.

II. THEORY

A. Basic formulations of SFG-VS for achiral surface

Sum frequency generation (SFG) is the second order nonlinear process when two photons at the frequency ω_1 and ω_2 simultaneously interact with a molecule to generate a photon with the frequency at the sum of the two

frequencies, *i.e.* $\omega = \omega_1 + \omega_2$. The special case for SFG, when $\omega_1 = \omega_2$ and from the same light beam, is called SHG. It has been known that because of the symmetry requirement, all the even order nonlinear processes, including the second order SFG process, are surface specific and can be used as surface selective probes [45]. In the SFG vibrational spectroscopy, ω_1 is usually fixed at a visible light frequency, and the SFG signal at ω is recorded at different ω_2 in the infrared frequencies. When the ω_2 is in resonance with the vibrational frequency of the interfacial molecules, the SFG signal is enhanced to give the spectroscopic response of the interfacial molecular vibrations [22,46]. The intensity of the SFG signal ($I(\omega)$) from a surface is proportional to the intensities of the incident visible and infrared light beams ($I(\omega_1)$ and $I(\omega_2)$, respectively), as well as the square of the effective susceptibility $\chi_{\text{eff}}^{(2)}$ of the interface [22,46].

$$I(\omega) = \frac{8\pi^3\omega^2\sec^2\beta}{c^3n_1(\omega)n_1(\omega_1)n_1(\omega_2)} \left| \chi_{\text{eff}}^{(2)} \right|^2 I(\omega_1)I(\omega_2) \quad (2)$$

where c is the speed of light in the vacuum, ω , ω_1 , and ω_2 are the frequencies of the SFG signal, visible, and IR laser beams, respectively. $n_j(\omega_i)$ is the refractive index of bulk medium j at frequency ω_i , β_i is the incident or reflect angle from interface normal of the i th laser beam, and $I(\omega_i)$ is the intensity of the SFG signal or the incident laser beams, respectively. Effective second-order susceptibility $\chi_{\text{eff}}^{(2)}$ can be expressed in the form of [46],

$$\chi_{\text{eff}}^{(2)} = \frac{[\hat{\mathbf{e}}(\omega) \cdot \mathbf{L}(\omega)] \cdot \chi_{ijk}^{(2)} : [\mathbf{L}(\omega_1) \cdot \hat{\mathbf{e}}(\omega_1)] \cdot [\mathbf{L}(\omega_2) \cdot \hat{\mathbf{e}}(\omega_2)]}{[\mathbf{L}(\omega_2) \cdot \hat{\mathbf{e}}(\omega_2)]} \quad (3)$$

here $\chi_{ijk}^{(2)}$ represents the macroscopic second order nonlinear susceptibility tensor elements of the interface; while the $\hat{\mathbf{e}}(\omega_i)$ and the $\mathbf{L}(\omega_i)$ are the unit polarization vector and the Fresnel factor at ω_i , respectively.

For an azimuthally isotropic interface formed by the achiral molecules (symmetry $C_{\infty v}$), there are only seven non-vanishing components in the total 27 macroscopic susceptibility tensors $\chi_{ijk}^{(2)}$. These nonzero components are $\chi_{xxx} = \chi_{yyy}$, $\chi_{xzx} = \chi_{yzy}$, $\chi_{zxx} = \chi_{zyy}$, and χ_{zzz} . The effective second-order susceptibility $\chi_{\text{eff}}^{(2)}$ in four different polarization combination are the linear combination of these $\chi_{ijk}^{(2)}$ tensors by expanding the Eq.(3) as follows [22]:

$$\begin{aligned} \chi_{\text{ssp}}^{(2)} &= L_{yy}(\omega)L_{yy}(\omega_1)L_{zz}(\omega_2) \sin \beta_2 \chi_{yyz} \\ \chi_{\text{sps}}^{(2)} &= L_{yy}(\omega)L_{zz}(\omega_1)L_{yy}(\omega_2) \sin \beta_1 \chi_{yzy} \\ \chi_{\text{pss}}^{(2)} &= L_{zz}(\omega)L_{yy}(\omega_1)L_{yy}(\omega_2) \sin \beta \chi_{zyy} \\ \chi_{\text{ppp}}^{(2)} &= L_{zz}(\omega)L_{xx}(\omega_1)L_{xx}(\omega_2) \sin \beta \cos \beta_1 \cos \beta_2 \chi_{zxx} - \\ &\quad L_{xx}(\omega)L_{xx}(\omega_1)L_{zz}(\omega_2) \cos \beta \cos \beta_1 \sin \beta_2 \chi_{xxz} - \\ &\quad L_{xx}(\omega)L_{zz}(\omega_1)L_{xx}(\omega_2) \cos \beta \sin \beta_1 \cos \beta_2 \chi_{xzx} + \\ &\quad L_{zz}(\omega)L_{zz}(\omega_1)L_{zz}(\omega_2) \sin \beta \sin \beta_1 \sin \beta_2 \chi_{zzz} \quad (4) \end{aligned}$$

With the laboratory coordinates defined as that z is along the surface normal, and the xy plane is the plane of interface, L_{ii} ($i=x, y, z$) is the Fresnel coefficient determined by the refractive index of the two bulk phase and the interface layer, and the incident and reflected angles [22,46,47]. The p polarization is within the xz plane, and the s polarization is perpendicular to the xz plane. The polarization combination ssp indicates that the SF signal, the visible beam, and the IR beam are in s, s, and p polarization, respectively, and so on.

B. Inclusion of the chiral elements for surface SFG

In the case of azimuthally symmetric interface formed by chiral molecules, the surface has a symmetry of C_{∞} instead of $C_{\infty v}$. Then there are six more non-vanishing chiral macroscopic susceptibility tensors [5,23,36]. These chiral elements are: χ_{xyz} , χ_{yxz} , χ_{zxy} , χ_{zyx} , χ_{xzy} , and χ_{yzx} . The contribution of these chiral elements to total effective sum frequency susceptibility are:

$$\begin{aligned} \chi_{\text{chiral}}^{(2)} &= \cos \Omega \cos \Omega_1 \sin \Omega_2 L_{zz}(\omega) L_{xx}(\omega_1) \cdot \\ &\quad L_{yy}(\omega_2) \sin \beta \cos \beta_1 \chi_{xzy} - \\ &\quad \cos \Omega \cos \Omega_1 \sin \Omega_2 L_{xx}(\omega) L_{zz}(\omega_1) \cdot \\ &\quad L_{yy}(\omega_2) \cos \beta \sin \beta_1 \chi_{xzy} + \\ &\quad \sin \Omega \cos \Omega_1 \cos \Omega_2 L_{yy}(\omega) L_{zz}(\omega_1) \cdot \\ &\quad L_{xx}(\omega_2) \sin \beta_1 \cos \beta_2 \chi_{yzz} + \\ &\quad \sin \Omega \cos \Omega_1 \cos \Omega_2 L_{yy}(\omega) L_{xx}(\omega_1) \cdot \\ &\quad L_{zz}(\omega_2) \cos \beta_1 \sin \beta_2 \chi_{yzz} - \\ &\quad \cos \Omega \sin \Omega_1 \cos \Omega_2 L_{xx}(\omega) L_{yy}(\omega_1) \cdot \\ &\quad L_{zz}(\omega_2) \cos \beta \sin \beta_2 \chi_{xyz} + \\ &\quad \cos \Omega \sin \Omega_1 \cos \Omega_2 L_{zz}(\omega) L_{yy}(\omega_1) \cdot \\ &\quad L_{xx}(\omega_2) \sin \beta \cos \beta_2 \chi_{zyx} \quad (5) \end{aligned}$$

Therefore, we have,

$$\begin{aligned} \chi_{\text{eff}}^{(2)} &= \left(\sin \Omega \cos \Omega_1 \chi_{\text{sps}}^{(2)} + \cos \Omega \sin \Omega_1 \chi_{\text{pss}}^{(2)} + \right. \\ &\quad \left. \cos \Omega \cos \Omega_1 \chi_{\text{pps}}^{(2)} \right) \sin \Omega_2 + \left(\sin \Omega \sin \Omega_1 \chi_{\text{ssp}}^{(2)} + \right. \\ &\quad \left. \sin \Omega \cos \Omega_1 \chi_{\text{spp}}^{(2)} + \cos \Omega \sin \Omega_1 \chi_{\text{pss}}^{(2)} + \right. \\ &\quad \left. \cos \Omega \cos \Omega_1 \chi_{\text{ppp}}^{(2)} \right) \cos \Omega_2 \quad (6) \end{aligned}$$

here the chiral SFG responses at polarization combinations of pps, spp, and psp are defined as $\chi_{\text{pps}}^{(2)}$, $\chi_{\text{spp}}^{(2)}$, and $\chi_{\text{psp}}^{(2)}$, respectively.

$$\begin{aligned} \chi_{\text{spp}}^{(2)} &= L_{yy}(\omega)L_{zz}(\omega_1)L_{xx}(\omega_2) \sin \beta_1 \cos \beta_2 \chi_{yzz}^{(2)} + \\ &\quad L_{yy}(\omega)L_{xx}(\omega_1)L_{zz}(\omega_2) \cos \beta_1 \sin \beta_2 \chi_{yzz}^{(2)} \\ \chi_{\text{pps}}^{(2)} &= L_{zz}(\omega)L_{xx}(\omega_1)L_{yy}(\omega_2) \sin \beta \cos \beta_1 \chi_{zxy}^{(2)} - \\ &\quad L_{xx}(\omega)L_{zz}(\omega_1)L_{yy}(\omega_2) \cos \beta \sin \beta_1 \chi_{xzy}^{(2)} \end{aligned}$$

$$\chi_{\text{ppsp}}^{(2)} = L_{zz}(\omega)L_{yy}(\omega_1)L_{xx}(\omega_2) \sin \beta \cos \beta_2 \chi_{zyx}^{(2)} - L_{xx}(\omega)L_{yy}(\omega_1)L_{zz}(\omega_2) \cos \beta \sin \beta_2 \chi_{xyz}^{(2)} \quad (7)$$

Here we group these terms with the polarization angle of the infrared optical field (Ω_2) because in the SFG experiment usually the detection is performed with the IR polarization fixed either at the s- ($\Omega_2=90^\circ$) or p- ($\Omega_2=0^\circ$) polarizations. Since the SFG-VS intensities can be normalized to that of z-cut quartz crystals, therefore, with these experimental measurements, the absolute values for the three chiral elements $\chi_{\text{ppps}}^{(2)}$, $\chi_{\text{spp}}^{(2)}$, $\chi_{\text{psp}}^{(2)}$ and the four non-chiral elements $\chi_{\text{sps}}^{(2)}$, $\chi_{\text{pss}}^{(2)}$, $\chi_{\text{ssp}}^{(2)}$, $\chi_{\text{ppp}}^{(2)}$ can be obtained.

III. EXPERIMENTAL METHODS FOR DETERMINATION OF THE CHIRAL AND ACHIRAL ELEMENTS

Here several experimental detection methods are to be discussed: (i) Direct measurement of the pure chiral elements is not only subject to significant experimental errors, but also incapable of obtaining the sign or phase information of the $\chi_{\text{chiral}}^{(2)}$ terms; (ii) Single polarization angle method can obtain the sign or relative phase of the $\chi_{\text{chiral}}^{(2)}$ and $\chi_{\text{achiral}}^{(2)}$ terms, but it is subject to significant experimental errors for determination the values for the smaller chiral terms; (iii) Two polarization angle method can obtain both the sign or relative phase and the most accurate values for the $\chi_{\text{chiral}}^{(2)}$ and $\chi_{\text{achiral}}^{(2)}$ terms.

A. Limitations on direct measurement of the pure chiral SFG intensity

Each of the seven terms appears in the Eq.(6) can be directly measured when the three polarization angles Ω_i are fixed. For example, when $\Omega_2=90^\circ$, $\Omega_1=0^\circ$, and $\Omega=0^\circ$, the chiral intensity of $|\chi_{\text{ppps}}^{(2)}|^2$ can be directly measured. However, since the chiral term is usually more than one orders of magnitude smaller than the large achiral terms [5,6,38-40], the $|\chi_{\text{sps}}^{(2)}|^2$ intensity is usually more than two orders of magnitude smaller than the achiral $|\chi_{\text{sps}}^{(2)}|^2$, $|\chi_{\text{pss}}^{(2)}|^2$, $|\chi_{\text{ppp}}^{(2)}|^2$, or $|\chi_{\text{ssp}}^{(2)}|^2$ intensities. Therefore, not only the sign of the chiral terms can not be determined, but also the value of the chiral terms are subject to significant experimental errors.

For example, let's assume $\chi_{\text{ppps}}^{(2)}=0.5$ and $\chi_{\text{sps}}^{(2)}=5$, then $|\chi_{\text{ppps}}^{(2)}|^2 = 0.25$ and $|\chi_{\text{sps}}^{(2)}|^2=25$. Let's assume that in the experimental measurement for determination of the value $|\chi_{\text{ppps}}^{(2)}|^2$, the polarization angle $\Omega = 0^\circ$ is subject to errors. Then we will see that the relative error brought by 1° error of the Ω is about 82% (for 1°) or -58% (for -1°), as listed in the Table I. Therefore, the exact value of the $I_{\text{ppps}} \propto |\chi_{\text{ppps}}^{(2)}|^2$ and $\chi_{\text{ppps}}^{(2)}$ can hardly be accurately determined under such situation. It is even

TABLE I The value for $|\chi_{\text{ppps}}^{(2)}|^2$ with $\chi_{\text{ppps}}^{(2)}=0.5$ and $\chi_{\text{sps}}^{(2)}=5$ with errors on the SF polarization angle Ω .

Error of Ω	-2°	-1°	0°	1°	2°
Value of $ \chi_{\text{ppps}}^{(2)} ^2$	0.023	0.106	0.25	0.455	0.72

more difficult in actual measurement since the relative strength of the chiral term is usually smaller than what we assumed.

B. Advantages and limitations on the single polarization angle method

In the single polarization angle (SPA) method, SFG signal is detected when the polarization of either the visible light or the SFG signal is varied while the polarization angles of the other two are fixed at either s- ($\Omega=90^\circ$) or p- ($\Omega=0^\circ$) polarization. According to the Eq.(6) and as listed in Table II, in the SPA method, the $\chi_{\text{eff}}^{(2)}$ is always the mixing of one chiral term and one achiral term. For example, when $\Omega_1=0^\circ$ and $\Omega_2=90^\circ$, one has

$$\chi_{\Omega\text{ps}}^{(2)} = \sin \Omega \chi_{\text{sps}}^{(2)} + \cos \Omega \chi_{\text{ppps}}^{(2)} \quad (8)$$

here $\chi_{\text{sps}}^{(2)}$ is an achiral term and $\chi_{\text{ppps}}^{(2)}$ is a chiral term. It is now clear that by varying the Ω , the SFG intensity which is proportional to $|\chi_{\Omega\text{ps}}^{(2)}|^2$ is the results of the polarization angle dependent interference between the achiral $\chi_{\text{sps}}^{(2)}$ term and the chiral $\chi_{\text{ppps}}^{(2)}$ term. Table II listed all such combinations in the single polarization angle (SPA) measurements when the IR polarization is fixed at 0° (p-polarization) or 90° (s-polarization).

One can immediately see the similarity of Eq.(10) with the polarization null angle (PNA) measurement technique for the achiral surface SFG-VS studies, where $\Omega_1=-45^\circ$ is fixed and the null angle (Ω^{null}) for the zero SFG-VS intensity is determined [22,25,30]. Here from Eq.(10), one can easily show that when $\chi_{\Omega^{\text{null}}\text{ps}}^{(2)}=0$, then one has $\tan \Omega^{\text{null}} = \sin \Omega^{\text{null}} / \cos \Omega^{\text{null}} = -\chi_{\text{ppps}}^{(2)} / \chi_{\text{sps}}^{(2)}$. Therefore, if the polarization null angle (PNA) can be accurately measured in this SPA approach, the relative sign and accurate ratio between the chiral and achiral terms, such as $\chi_{\text{ppps}}^{(2)}$ and $\chi_{\text{sps}}^{(2)}$ can be quite accurately determined. Similar results can be readily obtained for other cases as listed in the Table II.

However, there is a catch. We already know that in general the chiral term is more than one order of magnitude smaller than that of the achiral term [5,6,38-40]. Assume again $\chi_{\text{ppps}}^{(2)}=0.5$ and $\chi_{\text{sps}}^{(2)}=5$, since $\arctan -0.1 = -5.7^\circ$, this means that all the null angle measured in this approach is going to be within the range between -5.7° and 5.7° . This is still a manageable problem if the accuracy of the null angle measurement can be significantly improved to be significantly

TABLE II Two ways of applying the SPA method. In order to distinguish the chiral terms from the non-chiral terms, all the chiral terms are all listed as a second term.

Varying the visible polarization angle Ω_1				Varying the SF polarization angle Ω			
SFG(Ω)	Vis(Ω_1)	IR(Ω_2)	$\chi_{\text{eff}}^{(2)}$	SFG(Ω)	Vis(Ω_1)	IR (Ω_2)	$\chi_{\text{eff}}^{(2)}$
0°(p)	Ω_1	90°(s)	$\sin \Omega_1 \chi_{\text{pss}}^{(2)} + \cos \Omega_1 \chi_{\text{pps}}^{(2)}$	Ω	0°(p)	90°(s)	$\sin \Omega \chi_{\text{sps}}^{(2)} + \cos \Omega \chi_{\text{pps}}^{(2)}$
0°(p)	45°	90°(s)	$(\chi_{\text{pss}}^{(2)} + \chi_{\text{pps}}^{(2)})/\sqrt{2}$	45°	0°(p)	90°(s)	$(\chi_{\text{sps}}^{(2)} + \chi_{\text{pps}}^{(2)})/\sqrt{2}$
0°(p)	-45°	90°(s)	$(-\chi_{\text{pss}}^{(2)} + \chi_{\text{pps}}^{(2)})/\sqrt{2}$	-45°	0°(p)	90°(s)	$(-\chi_{\text{sps}}^{(2)} + \chi_{\text{pps}}^{(2)})/\sqrt{2}$
0°(p)	Ω_1	0°(p)	$\cos \Omega_1 \chi_{\text{ppp}}^{(2)} + \sin \Omega_1 \chi_{\text{psp}}^{(2)}$	Ω	0°(p)	0°(p)	$\cos \Omega \chi_{\text{ppp}}^{(2)} + \sin \Omega \chi_{\text{spp}}^{(2)}$
0°(p)	45°	0°(p)	$(\chi_{\text{ppp}}^{(2)} + \chi_{\text{psp}}^{(2)})/\sqrt{2}$	45°	0°(p)	0°(p)	$(\chi_{\text{ppp}}^{(2)} + \chi_{\text{spp}}^{(2)})/\sqrt{2}$
0°(p)	-45°	0°(p)	$(\chi_{\text{ppp}}^{(2)} - \chi_{\text{psp}}^{(2)})/\sqrt{2}$	-45°	0°(p)	0°(p)	$(\chi_{\text{ppp}}^{(2)} - \chi_{\text{spp}}^{(2)})/\sqrt{2}$
90°(s)	Ω_1	0°(p)	$\sin \Omega_1 \chi_{\text{ssp}}^{(2)} + \cos \Omega_1 \chi_{\text{sp}p}^{(2)}$	Ω	90°(s)	0°(p)	$\sin \Omega \chi_{\text{ssp}}^{(2)} + \cos \Omega \chi_{\text{sp}p}^{(2)}$
90°(s)	45°	0°(p)	$(\chi_{\text{ssp}}^{(2)} + \chi_{\text{sp}p}^{(2)})/\sqrt{2}$	45°	90°(s)	0°(p)	$(\chi_{\text{ssp}}^{(2)} + \chi_{\text{sp}p}^{(2)})/\sqrt{2}$
90°(s)	-45°	0°(p)	$(-\chi_{\text{ssp}}^{(2)} + \chi_{\text{sp}p}^{(2)})/\sqrt{2}$	-45°	90°(s)	0°(p)	$(-\chi_{\text{ssp}}^{(2)} + \chi_{\text{sp}p}^{(2)})/\sqrt{2}$

less than one degree. Therefore, the SPA method certainly is advantageous in terms of obtaining the sign or relative phase, as well as the relative intensity of all the chiral and achiral terms in the SFG measurement.

Furthermore, there is still another catch in the SPA approach. The SPA method is not made for accurately measuring the DCE values. Figure 2 plotted the simulation of the $|\chi_{\Omega_{\text{ps}}}^{(2)}|^2$ vs. Ω with $\chi_{\text{pps}}^{(2)}=0.5$ and $\chi_{\text{sps}}^{(2)}=5$, and the simulation with $|\chi_{\Omega_{\text{ps}}}^{(2)}|^2$ vs. Ω_1 with $\chi_{\text{pps}}^{(2)}=0.5$ and $\chi_{\text{pss}}^{(2)}=10$.

For the case of $|\chi_{\Omega_{\text{ps}}}^{(2)}|^2$ vs. Ω , one has,

$$I_{45^\circ\text{ps}} \propto |\chi_{45^\circ\text{ps}}^{(2)}|^2 = \frac{1}{2} |\chi_{\text{sps}}^{(2)} + \chi_{\text{pps}}^{(2)}|^2 \quad (9)$$

$$I_{-45^\circ\text{ps}} \propto |\chi_{-45^\circ\text{ps}}^{(2)}|^2 = \frac{1}{2} |\chi_{\text{sps}}^{(2)} - \chi_{\text{pps}}^{(2)}|^2 \quad (10)$$

It is clear that since $\chi_{\text{sps}}^{(2)} \gg \chi_{\text{pps}}^{(2)}$, the difference $I_{45^\circ\text{ps}} - I_{-45^\circ\text{ps}}$ is always small, and the DCE value as defined in the Eq.(1) can be small. Here we can have an estimate the upper limit of the DCE values. For $\chi_{\text{pps}}^{(2)}=0.5$ and $\chi_{\text{sps}}^{(2)}=5$, DCE=39.6%; while for $\chi_{\text{pps}}^{(2)}=0.5$ and $\chi_{\text{pss}}^{(2)}=10$, DCE=20.0%. Since both $I_{45^\circ\text{ps}}$ and $I_{-45^\circ\text{ps}}$ are on the steepest part of the $|\chi_{\Omega_{\text{ps}}}^{(2)}|^2$ vs. Ω curve as illustrated in Fig.2, the uncertainty in the experimental measurement of the DCE value is going to be significantly large. As discussed previously in the quantitative DCE measurement with SHG-LD [9], the similarly shaped p-detection curve in general has an error bar of ~10% or more for the DCE value. Considering the fact that usually in the SHG-LD measurement, better signal/noise ratio can be achieved than that in the SFG measurement, the error bar in the SFG-VS measurement can be significantly larger than 10%. This would make it difficult to measure the DCE value accurately using the SPA method in SFG-VS. Usually the DCE value is significantly smaller than the upper limit as estimated above. It is often likely that the error bar can exceed the largest DCE value one can measure from

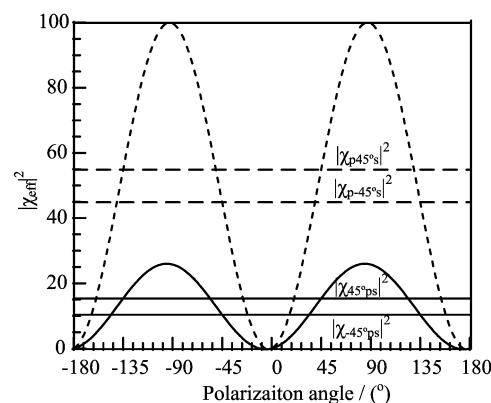


FIG. 2 Simulation results of the SPA method. Dashed curve: $|\chi_{\text{p}\Omega_{1\text{s}}}^{(2)}|^2$ vs. Ω_1 with $\chi_{\text{pps}}^{(2)}=0.5$ and $\chi_{\text{pss}}^{(2)}=10$; Solid curve: $|\chi_{\Omega_{\text{ps}}}^{(2)}|^2$ vs. Ω with $\chi_{\text{pps}}^{(2)}=0.5$ and $\chi_{\text{sps}}^{(2)}=5$. On both curves the intensity difference at the 45° and -45° is not apparent.

the SPA experiment. Therefore, even the surface is chiral, one may not be able to make such conclusion from the SPA measurement. This is certainly the limitation for the SPA measurement in the chiral surface studies.

In summary, the SPA approach does have much more advantages over the pure chiral elements detection method, the influences from the polarization angle errors still remarkable. However, its application in determination of the surface chirality is significantly limited.

C. Accurate determination of surface chirality with the TPA method

Here we show that the unique accuracy and sensitivity for surface chirality measurement with the s-polarization detection in the SHG-LD can be realized with the so called TPA approach. It is also interesting to note that various schemes in the TPA approach can be selected and designed for accurate surface chirality

measurement.

In the SHG-LD s-polarization detection, the uniqueness comes from the $\cos^2 \Omega$ and $\sin 2\Omega$ functions are associated with the chiral and achiral terms, respectively, as showing in the Eq.(13). Because the achiral term is much larger than the chiral term, then the maximum intensity is going to be around $\Omega=\pm 45^\circ$, and the interference between the chiral and achiral terms are going to be maximized around $\Omega=\pm 45^\circ$. This shall not only allow direct recognition of the surface chirality by looking at the different SHG intensities at the $\Omega=45^\circ$ and $\Omega=-45^\circ$, but also allow accurate determination of the DCE value.

$$I_s^{\text{SHG}}(\Omega) \propto |\chi_{\text{eff},s}^{(2)}(\Omega)|^2 = |\chi_{\text{chiral}}^{(2)} \cos^2 \Omega + \chi_{45^\circ s}^{(2)} \sin 2\Omega|^2 \quad (11)$$

One simplest way to make the SFG-VS-LD similar to the SHG-LD is to have $\Omega_2=90^\circ$ and let $\Omega_1=\pm\Omega$. Thus, one has,

$$I_{\pm}^{\text{S}}(\Omega) \propto |\chi_{\text{eff}}^{(2)}(\Omega)|^2 = \left| \chi_{\text{pps}}^{(2)} \cos^2 \Omega + \frac{1}{2}(\chi_{\text{sps}}^{(2)} \pm \chi_{\text{pss}}^{(2)}) \sin 2\Omega \right|^2 \quad (12)$$

Another option is to have $\Omega_2=0^\circ$ and let $\Omega_1 \pm \Omega=90^\circ$. One has,

$$I_{\pm}^{\text{P}}(\Omega) \propto |\chi_{\text{eff}}^{(2)}(\Omega)|^2 = \left| \chi_{\text{psp}}^{(2)} \cos^2 \Omega \pm \chi_{\text{spp}}^{(2)} \sin^2 \Omega + \frac{1}{2}(\chi_{\text{ssp}}^{(2)} \pm \chi_{\text{ppp}}^{(2)}) \sin 2\Omega \right|^2 \quad (13)$$

The reason not to have the two cases of $\Omega_2=90^\circ$ with $\Omega_1 \pm \Omega=90^\circ$ and $\Omega_2=0^\circ$ with $\Omega_1=\pm\Omega$ is that in these two cases the $\cos^2 \Omega$ and $\sin^2 \Omega$ terms are associated with the achiral susceptibility terms, while the $\sin 2\Omega$ term is associated with the chiral susceptibility terms. In this two cases, the surface chirality is not going to be explicit and the DCE values shall be subject to large experimental errors.

Figure 3 illustrates the simulation results for $I_{\pm}^{\text{P}}(\Omega)$ and $I_{\pm}^{\text{S}}(\Omega)$ with the following values for the chiral and achiral susceptibility tensors: $\chi_{\text{pps}}^{(2)}=0.5$, $\chi_{\text{spp}}^{(2)}=1$, $\chi_{\text{psp}}^{(2)}=0.5$, $\chi_{\text{sps}}^{(2)}=5$, $\chi_{\text{pss}}^{(2)}=10$, $\chi_{\text{ssp}}^{(2)}=10$, $\chi_{\text{ppp}}^{(2)}=20$. The choosing of these values are rather arbitrary except making the chiral susceptibility terms much smaller than the achiral susceptibility terms. Also, the choice of the values is also in general agreement with the fact that the ssp and ppp intensities in the SFG-VS measurement are usually larger than the sps and pss intensities.

It is clear that the $I_{+}^{\text{P}}(\Omega)$ and $I_{+}^{\text{S}}(\Omega)$ curves have larger SFG intensities and also larger chiral modulations at the

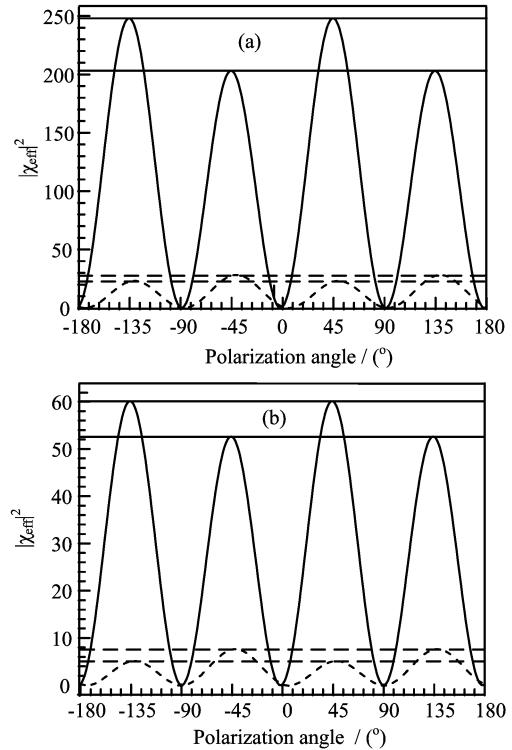


FIG. 3 TPA simulation results with $\chi_{\text{pps}}^{(2)}=0.5$, $\chi_{\text{spp}}^{(2)}=1$, $\chi_{\text{psp}}^{(2)}=0.5$, $\chi_{\text{sps}}^{(2)}=5$, $\chi_{\text{pss}}^{(2)}=10$, $\chi_{\text{ssp}}^{(2)}=10$, $\chi_{\text{ppp}}^{(2)}=20$. (a) Solid curve: $I_{+}^{\text{P}}(\Omega)=I_{\Omega,90-\Omega,0^\circ}$; dashed curve: $I_{-}^{\text{P}}(\Omega)=I_{\Omega,90+\Omega,0^\circ}$. (b) Solid curve: $I_{+}^{\text{S}}(\Omega)=I_{\Omega,\Omega,90^\circ}$; dashed curve: $I_{-}^{\text{S}}(\Omega)=I_{\Omega,-\Omega,90^\circ}$. The horizontal lines are indicators of $|\chi_{\text{eff}}^{(2)}(-45^\circ)|^2$ and $|\chi_{\text{eff}}^{(2)}(45^\circ)|^2$ values.

peaks around $\Omega=\pm 45^\circ$. This effect contributes to the same signs of achiral susceptibility pairs $\chi_{\text{ssp}}^{(2)}/\chi_{\text{ppp}}^{(2)}$ and $\chi_{\text{sps}}^{(2)}/\chi_{\text{pss}}^{(2)}$. Reciprocally, from the relative magnitude of the SFG peak signal strengths for the $I_{-}(\Omega)$ and $I_{+}(\Omega)$ curves, we can directly tell whether the $\chi_{\text{ssp}}^{(2)}/\chi_{\text{ppp}}^{(2)}$ pair or the $\chi_{\text{sps}}^{(2)}/\chi_{\text{pss}}^{(2)}$ pair have the same or opposite signs.

It is to be noted that in above discussion we only treat all the susceptibility tensors as real numbers. This is based on the assumption that these tensors all have the same or opposite signs. It is indeed true for most of dielectric molecular surface layers [37].

In the sections below, we shall show that the SFG-VS TPA measurements on the chiral S- and R-lemonene liquid surfaces are in good agreement with the formulation and discussions above on the TPA methods.

IV. EXPERIMENTS

The setup of the SFG-VS experiment was the same as in previous reports [28,48,49]. The 10 Hz and 23 ps SFG spectrometer laser system was purchased from EKSPILA, using a co-propagating configuration. Some of the SFG polarization optics were rearranged from the

original design by EKSPLA to improve the polarization control in the SFG experiment [33]. The incident angle of the visible beam is 63° (β_1) and it is 50° (β_2) for the IR beam. The SFG signal was collected around 62° (β) at the reflection geometry. To perform the SPA detection, the visible wavelength was fixed at 532.1 nm and the IR beam was tuned from 2800 cm^{-1} to 3000 cm^{-1} with a 2 cm^{-1} increment. The signal for each point was averaged over 700–900 laser pulses. To perform the TPA experiment, the wavelength of the IR beam was set at a specific value and the SFG signal was recorded when the polarization angles of visible beam and SFG signal were varied. The increment of polarization angles in this experiment was 8° per step and adjusted manually. Therefore, the signal/noise ratio can be significantly improved if such procedure is automated and computer controlled. The signal at each point was averaged over 300 pulses. The spectrum intensity was normalized to the intensities of the corresponding visible and IR laser pulses, and then to the z -cut α -quartz surface signal to obtain the absolute value of the surface SFG response. The details of the normalization procedure were described previously [33].

All SFG-VS measurements were carried out at controlled room temperature ($22.0 \pm 0.5^\circ\text{C}$) and humidity ($\sim 40\%$). The liquid samples were filled in a round Teflon beaker with diameter of $\sim 5\text{ cm}$. The S- and R-limonene liquid samples were purchased from Aldrich. The purities are $\geq 98.0\%$ (sum of enantiomorphs, GC) for R-limonene and $\geq 96.0\%$ (sum of enantiomorphs, GC) for S-limonene. Although it was reported that the limonene molecule can be oxidized in the moist air, there was no noticeable change of the SFG-VS signal during 2 h of exposure to the air with humidity of $\sim 40\%$.

V. RESULTS

A. Chiral SFG-VS spectra of the S- and R-limonene air/liquid surface

The chiral SFG-VS spectra of the S- and R-limonene bulk liquid were reported by Belkin *et al.* previously [6,50]. However, no surface chiral SFG-VS spectra of S- and R-limonene has been reported to our knowledge so far.

In Fig.4, the normalized surface SFG-VS chiral spectra ($\Delta I = I_{p45^\circ p} - I_{p-45^\circ p}$) of S- and R-limonene air/liquid surfaces are presented. There are two apparent spectral peaks around 2835 and 2880 cm^{-1} , and possibly a weak peak around 2920 cm^{-1} can be identified from the spectra. These peaks are in agreement with the reported chiral SFG-VS spectra peaks measured for the pure chiral bulk liquids [50]. However, the relative strengths of these peaks are different due to reasons unknown to us so far.

The two $\Delta I = I_{p45^\circ p} - I_{p-45^\circ p}$ spectra for the S- and R-limonene are almost mirror image to each other. This

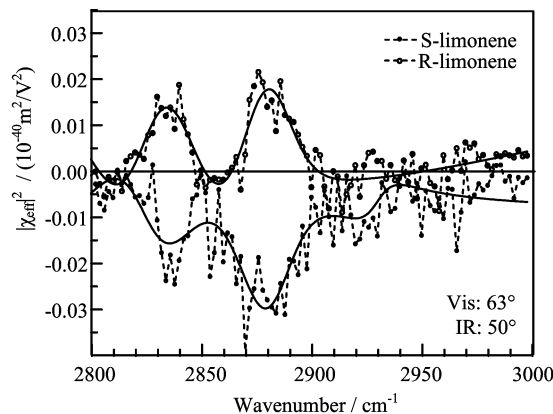


FIG. 4 The chiral SFG-VS spectra for S- and R-limonene as obtained using the SPA measurement. The vertical axis is the normalized absolute value for the $\Delta I = I_{p45^\circ p} - I_{p-45^\circ p}$. The chiral spectra indicates that there are three chiral vibrational bands in the $2800\text{--}3000\text{ cm}^{-1}$ region, *i.e.* 2835 , 2880 cm^{-1} , and possibly the 2920 cm^{-1} bands.

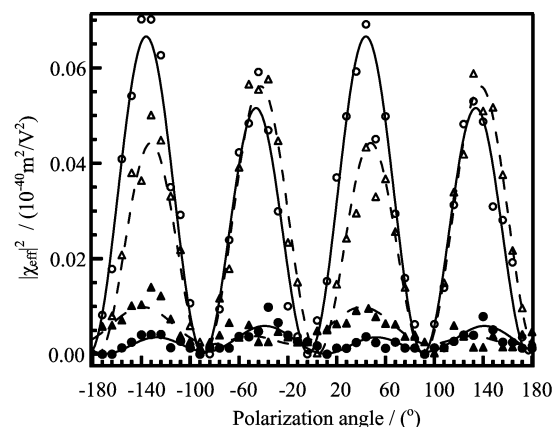


FIG. 5 $I_{\pm}^P(\Omega)$ TPA results of S- and R-limonene air/liquid surfaces at 2880 cm^{-1} . The vertical axis is the normalized absolute value for $I_{\pm}^P(\Omega)$. Solid circle with solid line: $I_{\pm}^P(\Omega)$ for R-limonene, open circle with solid line: $I_{+}^P(\Omega)$ for R-limonene, solid triangle with dashed line: $I_{\pm}^P(\Omega)$ for S-limonene, and open triangle with dashed line: $I_{+}^P(\Omega)$ for S-limonene.

indicates the chiral nature of the SFG-VS spectra was obtained.

B. Accurate DCE measurement with the TPA method

TPA measurement was performed for the three chiral peaks at 2835 , 2880 , and 2920 cm^{-1} . Here only the $I_{\pm}^P(\Omega)$ results for the 2880 cm^{-1} are presented in Fig.5. The $I_{\pm}^S(\Omega)$ curves have much smaller SFG intensities and signal/noise ratio. This is because that the sps and pss terms are relatively small in comparison to the ssp and ppp terms.

The polarization dependent $I_{\pm}^P(\Omega)$ TPA curves be-

TABLE III Calculated DCE values as well as the susceptibility tensor elements from the TPA data as in the Fig.3 for the 2835, 2880, and 2920 cm^{-1} peaks. The TPA data for the 2835 and 2920 cm^{-1} peaks are not shown. The unit of the susceptibilities is 10^{-20}m/V .

Limone		2835 cm^{-1}	2880 cm^{-1}	2920 cm^{-1}
R	DCE ₋	-6.4±5.0%	-53.1±15.0%	-7.0±1.4%
	DCE ₊	25.1±0.9%	25.4±1.3%	11.6±0.8%
S	DCE ₋	-15.5±7.9%	84.8±55.0%	4.3±0.2%
	DCE ₊	-25.9±2.3%	-23.7±0.4%	-9.1±0.8%
R	$\chi_{\text{ppp}}^{(2)}$	0.26±0.06	0.29±0.01	0.25±0.05
	$\chi_{\text{ssp}}^{(2)}$	0.28±0.06	0.20±0.01	0.38±0.03
	$\chi_{\text{spp}}^{(2)}$	0.01±0.02	0.004±0.01	0.001±0.01
	$\chi_{\text{psp}}^{(2)}$	0.03±0.02	0.03±0.01	0.02±0.01
S	$\chi_{\text{ppp}}^{(2)}$	0.24±0.01	0.30±0.02	0.21±0.02
	$\chi_{\text{ssp}}^{(2)}$	0.30±0.01	0.20±0.02	0.40±0.01
	$\chi_{\text{spp}}^{(2)}$	0.01±0.02	0.02±0.01	0.02±0.01
	$\chi_{\text{psp}}^{(2)}$	-0.05±0.02	-0.05±0.01	-0.03±0.01

haved just as predicted by the theoretical treatment and simulation in the Section III. The fitting results of these TPA curves with the Eq.(15) as well as the calculated DCE values using Eq.(1) are listed in the Table III.

According to these results, the following conclusions can be made. (i) The DCE values obtained from the $I_{+}^{\text{P}}(\Omega)$ curves are accurate. This is because the ssp and ppp terms are with the same sign, and thus the $I_{+}^{\text{P}}(\Omega)$ signals are much stronger. The error bar for DCE thus obtained is only $\sim 1\%$. This indicates that the TPA method can be used to accurately measure the chirality of chiral surfaces. Considering the fact that the polarization angle was manually adjusted in our experiment, much better data quality and less experimental error can be achieved when automation and computer controls are introduced. (ii) The DCE values for the S- and R-lemonene are almost identical in magnitude but opposite in sign from the more accurate DCE₊ values. This suggests that the surface structure of the S- and R-Limonene are indeed similar. (iii) The absolute values for the ssp, ppp, psp, and spp susceptibility tensors for the S- and R-limonene air/liquid surfaces are obtained directly from the TPA measurement. The spp term value is small and below the error level. This suggests that the TPA approach can be used as a standard technique for measurement of the nonlinear susceptibilities for the molecular surfaces.

In summary, here the experimental results clearly demonstrated the effectiveness of the TPA method in the SFG-VS-LD. Detail analysis and interpretations of the SFG spectra and TPA data of S- and R-limonene shall be reported in future works.

VI. CONCLUSION AND PERSPECTIVE

In this report, we discussed several SFG-VS-LD methods, and demonstrated their applicabilities in surface chirality studies. With SFG-VS experimental data on the S- and R-limonene air/liquid interface molecule, the effectiveness and efficiency of the TPA method are demonstrated. The TPA method is proven to be able to accurately measure the absolute values of the chiral and achiral susceptibility tensor elements of the molecular interface. It can also accurately determine the DCE of the molecular interface. With such accuracy, SFG-VS-LD technique can be used to study the details of chiral molecular recognition at molecular surfaces, as well as biological membranes.

The TPA method also need to be further developed to test different possibilities as well as for various applications. Expansion of the TPA method into molecular surfaces other than the $C_{\infty v}$ and C_{∞} symmetries is also useful for studying ordered surfaces and meta-materials. Application of the TPA method into double resonance SFG-VS can also be used to probe the electronic excited states as well as the high-vibrational ground states [51] as well as the chiral electronic coupling in the molecules [52].

The application of the TPA method is not necessarily restricted in chiral detection at liquid interface. It can be applied universally measuring the values and relative phases of any susceptibilities at four polarization combinations, especially the susceptibilities of the solid surface. Combined with automatic polarization modulating techniques, the SFG-VS TPA method can achieve much better polarization angular resolution, faster data acquisition rate, and better accuracy. Combining with the recent development of the broad-band SFG technology, the SFG-VS TPA technique can be even more powerful technique for interrogating the details in the chiral and achiral molecular interfaces. For example, in combining with the molecular computation studies, these detailed knowledge on the nonlinear optical properties of the chiral molecules may be used to determine absolute chiral structure of molecules. We are looking forward to its further development and applications in diverse areas.

VII. ACKNOWLEDGMENTS

Hong-fei Wang thanks the support by the Natural Science Foundation of China (NSFC) (No.20373076, No.20425309, and No.20533070) and the Ministry of Science and Technology of China (MOST) (No.2007CB815205). Shi-lin Liu thanks the support by the NSFC (No.20533070) and the MOST (No.2007CB815204). Yuan Guo thanks the support by the NSFC (No.20673122) and the MOST (No.2007CB815205).

- [1] J. D. Byers, H. I. Yee, T. Petralli-mallow, and J. M. Hicks, *Phys. Rev. B* **49**, 14643 (1994).
- [2] M. Kauranen, T. Verbiest, E. W. Meijer, E. E. Havinga, M. N. Teerenstra, A. J. Schouten, R. J. M. Nolte, and A. Persoons, *Adv. Mater.* **7**, 641 (1995).
- [3] S. Sioncke, T. Verbiest, and A. Persoons, *Mater. Sci. Eng. R* **42**, 115 (2003).
- [4] M. A. Kriech and J. C. Conboy, *J. Opt. Soc. Am. B* **21**, 1013 (2004).
- [5] P. Fischer and F. Hache, *Chirality* **17**, 421 (2005).
- [6] M. A. Belkin and Y. R. Shen, *Int. Rev. Phys. Chem.* **24**, 257 (2005).
- [7] G. J. Simpson, *ChemPhysChem* **5**, 1301 (2004).
- [8] X. Y. Chen, M. L. Clarke, J. Wang, and Z. Chen, *Int. J. Mod. Phys. B* **19**, 691 (2005).
- [9] Y. Y. Xu, Y. Rao, D. S., Zheng, Y. Guo, M. H. Liu, and H. F. Wang, *J. Phys. Chem. C* **113**, 4088 (2009).
- [10] Y. R. Shen, *Ann. Rev. Mat. Sci.* **16**, 69 (1986).
- [11] G. L. Richmond, J. M. Robinson, and V. L. Shannon, *Prog. Surf. Sci.* **28**, 1 (1988).
- [12] Y. R. Shen, *Nature* **337**, 519 (1989).
- [13] Y. R. Shen, *Annu. Rev. Phys. Chem.* **40**, 327 (1989).
- [14] J. A. Giordmaine, *Phys. Rev.* **138**, A1599 (1965).
- [15] L. D. Barron and A. D. Buckingham, *Mol. Phys.* **20**, 1111 (1971).
- [16] L. D. Barron, M. P. Bogaard, and A. D. Buckingham, *J. Am. Chem. Soc.* **95**, 603 (1973).
- [17] E. Charney, *The Molecular Basis of Optical Activity*. New York: John Wiley & Sons, (1979).
- [18] N. Berova, K. Nakanishi, and R. W. Woody, *Circular Dichroism: Principles and Applications*. New York: John Wiley & Sons, (2002).
- [19] L. A. Nafie, *Ann. Rev. Phys. Chem.* **48**, 357 (1997).
- [20] L. A. Nafie, T. B. Freedman, In: *Circular Dichroism: Principles and Applications*, 2nd edn. K. Nakanishi, N. Berova, R. Woody, Eds, New York: Wiley, 97 (2000).
- [21] L. D. Barron, *Molecular Light Scattering and Optical Activity*, 2nd edn. Cambridge: Cambridge University Press, (2004).
- [22] H. F. Wang, W. Gan, R. Lu, Y. Rao, and B. H. Wu, *Int. Rev. Phys. Chem.* **24**, 191 (2005).
- [23] W. K. Zhang, H. F. Wang, and D. S. Zheng, *Phys. Chem. Chem. Phys.* **8**, 4041 (2006).
- [24] Y. Rao, Y. S. Tao, and H. F. Wang, *J. Chem. Phys.* **119**, 5226 (2003).
- [25] R. Lu, W. Gan, and H. F. Wang, *Chin. Sci. Bull.* **48**, 2183 (2003).
- [26] R. Lu, W. Gan, and H. F. Wang, *Chin. Sci. Bull.* **49**, 899 (2004).
- [27] H. F. Wang, *Chin. J. Chem. Phys.* **17**, 362 (2004).
- [28] R. Lu, W. Gan, B. H. Wu, H. Chen, and H. F. Wang, *J. Phys. Chem. B* **108**, 7297 (2004).
- [29] M. A. Polizzi, R. M. Plocinik, and G. J. Simpson, *J. Am. Chem. Soc.* **126**, 5001 (2004).
- [30] W. Gan, B. H. Wu, H. Chen, Y. Guo, and H. F. Wang, *Chem. Phys. Lett.* **406**, 467 (2005).
- [31] R. Lu, W. Gan, B. H. Wu, Z. Zhang, Y. Guo, and H. F. Wang, *J. Phys. Chem. B* **109**, 14118 (2005).
- [32] W. Gan, D. Wu, Z. Zhang, and H. F. Wang, *Chin. J. Chem. Phys.* **19**, 20 (2006).
- [33] W. Gan, D. Wu, Z. Zhang, R. R. Feng, and H. F. Wang, *J. Chem. Phys.* **124**, 114705 (2006).
- [34] N. J. Begue, A. J. Moad, and G. J. Simpson, *J. Phys. Chem. C* **113**, 10158 (2009).
- [35] N. J. Begue, R. M. Everly, V. J. Hall, L. Hauptert, and G. J. Simpson, *J. Phys. Chem. C* **113**, 10166 (2009).
- [36] A. J. Moad and G. J. Simpson, *J. Phys. Chem. B* **108**, 3548 (2004).
- [37] D. S. Zheng, Y. Wang, A. A. Liu, H. F. Wang, *Int. Rev. Phys. Chem.* **27**, 629 (2008).
- [38] P. Fischer, D. S. Wiersma, R. Righini, B. Champagne, and A. D. Buckingham, *Phys. Rev. Lett.* **85**, 4253 (2000).
- [39] P. Fischer, A. D. Buckingham, and A. C. Albrecht, *Phys. Rev. A* **64**, 053816 (2001).
- [40] D. S. Ji and Y. R. Shen, *Chirality* **18**, 146 (2006).
- [41] G. Martin-Gassin, E. Benichou, G. Bachelier, I. Russier-Antoine, C. Jonin, and B. F. Brevet, *J. Phys. Chem. C* **112**, 12958 (2008).
- [42] Y. Y. Xu, F. Wei, and H. F. Wang, *J. Phys. Chem. C* **113**, 4222 (2009).
- [43] G. Martin-Gassin, E. Benichou, G. Bachelier, I. Russier-Antoine, Ch. Jonin, and B. F. Brevet, *J. Phys. Chem. C* **113**, 4227 (2009).
- [44] T. Verbiest, M. Kauranen, J. J. Maki, M. N. Teerenstra, A. J. Schouten, R. J. M. Nolte, and A. Persoons, *J. Chem. Phys.* **103**, 8296 (1995).
- [45] Y. R. Shen, *The Principles of Nonlinear Optics*, New York: Wiley-Interscience, (1984).
- [46] X. W. Zhuang, P. B. Miranda, D. Kim, and Y. R. Shen, *Phys. Rev. B* **59**, 12632 (1999).
- [47] X. Wei, S. C. Hong, X. W. Zhuang, T. Goto, and Y. R. Shen, *Phys. Rev. E* **62**, 5160 (2000).
- [48] J. Feng, D. Wu, J. Wen, S. L. Liu, and H. F. Wang, *Chin. J. Chem. Phys.* **21**, 314 (2008).
- [49] Z. Zhang, D. S. Zheng, Y. Guo, and H. F. Wang, *Phys. Chem. Chem. Phys.* **11**, 991 (2009).
- [50] M. A. Belkin, T. A. Kulakov, K. H. Ernst, L. Yan, and Y. R. Shen, *Phys. Rev. Lett.* **85**, 4474 (2000).
- [51] D. Wu, G. H. Deng, Y. Guo, and H. F. Wang, *J. Phys. Chem. A* **113**, 6058 (2009).
- [52] M. A. Belkin and Y. R. Shen, *Phys. Rev. Lett.* **91**, 213907 (2003).